Sensors and Materials, Vol. 38, No. 2 (2026) 735–745
MYU Tokyo

S & M 4343

Proton Dose Dependence of Radio-photoluminescence Properties of Ag-doped Na–Al Phosphate Glasses

Hiroki Kawamoto,[1*] Masanori Koshimizu,[2] Kohtaku Suzuki,[3]
Go Okada,[4] Yutaka Fujimoto,[1] and Keisuke Asai[1]

[1]Department of Applied Chemistry, Graduate School of Engineering, Tohoku University, 6-6-07, Aoba, Aramaki, Aoba-ku, Sendai, Miyagi 980-8579, Japan
[2]Research Institute of Electronics, Shizuoka University, 3-5-1, Johoku, Chuouku, Hamamatsu 432-8011, Japan
[3]The Wakasa Wan Energy Research Center, 64-52-1, Nagatomi, Tsuruga, Fukui 914-0192, Japan
[4]Kanazawa Institute of Technology, 3-1 Yatsukaho, Hakusan, Ishikawa 924-0838, Japan

(Received October 27, 2025; accepted December 17, 2025)

Keywords: proton, dosimetry, radiophotoluminescence, Ag-doped phosphate glass

Ag-doped Na–Al phosphate glasses have been used in commercial personal dosimeters for X-rays, γ-rays, and β-rays owing to their radio-photoluminescence (RPL) properties. The RPL behavior in this material when irradiated with high-linear-energy-transfer (LET) radiation has been investigated; however, there are unclear points such as LET quenching. In this study, the proton (3.14 MeV, 22.1 keV/μm) dose dependence of the RPL properties of Ag-doped Na–Al phosphate glasses was investigated as a first step to elucidate the RPL mechanism under high-LET exposure. The optical absorption spectra suggested the formation of Ag^0, Ag^{2+}, Ag_3^{2+}, and the phosphorous–oxygen hole center (POHC) by proton irradiation. In the photoluminescence spectra with an excitation wavelength of 310 nm, broad emission peaking at 650 nm corresponding to Ag^{2+} and Ag_2^{+} was observed after proton irradiation. Furthermore, the formation of Ag^{2+}, Ag_2^{+}, POHC, and peroxy-radical by proton irradiation was revealed in the electron spin resonance spectra. Interestingly, the peroxy-radical signal in Ag-doped phosphate glasses has not been observed in previous studies where the glasses were irradiated with high doses of low-LET radiation, and it is possible that the peroxy-radical is formed only when the glasses are irradiated with high-LET radiation.

1. Introduction

Radio-photoluminescence[1,2] (RPL) is an emission phenomenon induced by the photoexcitation of luminescence centers (RPL centers) newly formed via exposure to ionizing radiation. RPL intensity increases with dose of ionizing radiation, reflecting an increase in the number of RPL centers formed. Hence, RPL is applied to the principle of luminescence-type dosimeters. In addition, RPL has several features that improve the convenience of using dosimeters. For example, the information of cumulative dose is not lost after readout and RPL centers are stable at ambient temperature and can be erased by heating at high temperatures.

*Corresponding author: e-mail: hiroki.kawamoto.c7@tohoku.ac.jp
https://doi.org/10.18494/SAM6006

ISSN 0914-4935

Owing to these features, dose information can be stored for a long time, repeatedly read out, and reset at will. Because of these advantages, RPL dosimeters are applied in fields such as personal dosimetry,[3] environmental monitoring,[4,5] medical dosimetry,[6] and dose imaging.[7,8]

Thus far, various RPL materials have been reported,[9] including MgF_2,[10] CaF_2,[11] Li_2CO_3,[12] Na_2CO_3,[13] $CaSO_4$,[14] Au-doped CsCl,[15] Au-doped soda-lime silicate glass,[16] Ag-doped phosphate glasses,[17,18] Ag-doped alkali halides,[19] Ag-doped borate glasses,[20,21] Cu-doped aluminoborosilicate glass,[22] Yb-doped NaCl,[23] Sm-doped $CaSO_4$,[24] Sm-doped HfO_2–Al_2O_3–SiO_2 glass ceramics,[25] Eu-doped CaF_2,[26] Eu-doped $NaMgF_3$ nanoparticles,[27] Tm-doped $NaMgF_3$,[28] Bi-doped $CaBPO_5$,[29] and Bi-doped $NaCaBO_3$.[30] Among these materials, Ag-doped phosphate glasses have been used in commercially available personal dosimeters as "glass badge". Since the RPL property of this glass was first reported in 1951,[31] the RPL property and mechanism have been investigated using various spectroscopic methods, such as ultraviolet–visible (UV–Vis) absorption, photoluminescence (PL), and electron spin resonance (ESR) spectroscopies.[32–35] The currently proposed RPL center formation mechanism is as follows.[36] First, electrons and holes are generated by ionizing radiation. Some electrons are trapped at Ag^+ and form Ag^0. Subsequently, Ag_2^+ clusters are formed by the association of Ag^+ and Ag^0. In contrast, some holes are trapped at PO_4^{3-} tetrahedra and form phosphorous–oxygen hole centers (POHCs). These trapped holes transfer to Ag^+, leading to the formation of Ag^{2+}. In addition, the formation of high-order Ag clusters such as Ag_3^{2+} and Ag_4^{2+} has been recently proposed.[37] Ag^0 emits blue (450 nm) RPL, whereas Ag^{2+} and Ag_2^+ emit orange (650 nm) RPL upon UV excitation.[34–36]

Ag-doped phosphate glasses are used in practical applications as dosimeters for low-linear-energy-transfer (LET) radiation such as X-rays, γ-rays, and β-rays, but their RPL properties when irradiated with high-LET radiation have also been investigated.[38–42] The LET dependence of the RPL response in Ag-doped phosphate glasses has been reported,[39–42] and some researchers revealed that the orange RPL efficiency decreased with the increase in LET value, which is called "LET quenching".[37,42] Recently, the possibility of the LET evaluation using these glasses has been demonstrated by LET quenching.[42] However, the origin of LET quenching remains unclear. To the best of our knowledge, UV–Vis absorption and PL spectra in the Ag-doped phosphate glasses when exposed to high-LET radiation have been reported, whereas ESR spectra have not been reported, and defects and chemical species including no-emission paramagnetic species formed by high-LET radiation have not yet been analyzed in detail. Therefore, we aimed to elucidate the RPL mechanism under high-LET radiation exposure. As a first step, in this study, we investigated the proton dose dependence of UV–Vis absorption, PL, and ESR spectra in Ag-doped phosphate glasses.

2. Experimental Methods

$27.72Na_2O$–$13.10Al_2O_3$–$59.09P_2O_5$–$0.09Ag_2O$ glass samples, which have the same composition as the commercially sold RPL glass (FD-7), were synthesized by the melt–quenching method in air. The raw materials, namely, $NaPO_3$ (99%, Kojundo), Na_2CO_3 (99.9%; Rare Metallic Co., Ltd.), $Al(PO_3)_3$ (99.99%; High Purity Chemicals Co., Ltd.), and Ag_2O (99.0%;

Wako Pure Chemical Industries Ltd.), were mixed, loaded into a platinum crucible, and melted at 1373 K in an electric furnace (FT-101, FULL-TECH. Co., Ltd.). The liquid melt was poured onto a stainless steel plate heated to 573 K, and then the melted liquid was cooled to room temperature in air. The obtained glasses were annealed at 723 K for 1 h, then cut into approximately 10 × 10 mm^2 and optically polished. To compare the absorbance values of the samples, the thickness of all the samples was 1 mm.

Proton irradiation in air at ambient temperature was performed at irradiation room 1 of Wakasa Wan Energy Research Center,[43] Fukui, Japan. The proton energy in vacuum was 3.4 MeV, and the proton beam was irradiated onto the samples through a 1 μm silicon nitride thin window and atmosphere, in the same way as in a previous report.[44] The irradiation energy in this case was determined to be 3.14 MeV by using a silicon surface detector. Prior to the proton irradiation experiment, the stopping range and LET of protons in Ag-doped phosphate glass were estimated using the Stopping and Range of Ions in Matter.[45] In Ag-doped phosphate glasses with the atomic ratio of Na: 11.12, Al: 6.17, P: 31.94, O: 50.61, and Ag: 0.17 and the density of 2.56 g/cm^3, the projected length and LET for the 3.14 MeV proton were estimated to be 85.3 μm and 22.1 keV/μm, respectively. From these estimations, 7.23 × 10^7 protons/cm^2 irradiation is needed for 1 Gy irradiation. A photograph of an area near the irradiation port is shown in Fig. 1(a). The slide glass mounting the samples [Fig. 1(b)] was attached to the moving stage. The stage was moved while the sample's position was remotely confirmed using a camera installed on the opposite side of the irradiation port, and irradiation was performed with the sample positioned in front of the irradiation port. Each different sample was irradiated with 1, 10, 100, 1000, or 10000 Gy.

To investigate the RPL properties, UV–Vis absorption, PL, and ESR spectra were measured at each dose. Since all the measurements were carried out after at least three days from proton irradiation, the progression of RPL center formation reaction with time elapsed at room temperature, known as the build-up effect, was negligible. UV–Vis absorption spectra in the range of 200–800 nm were measured using a spectrometer (UV-2700, Shimadzu). The PL spectra with the excitation wavelength of 310 nm and PL excitation (PLE) spectra with the emission wavelength of 650 nm were measured with a spectrometer (F-7000, Hitachi). The ESR

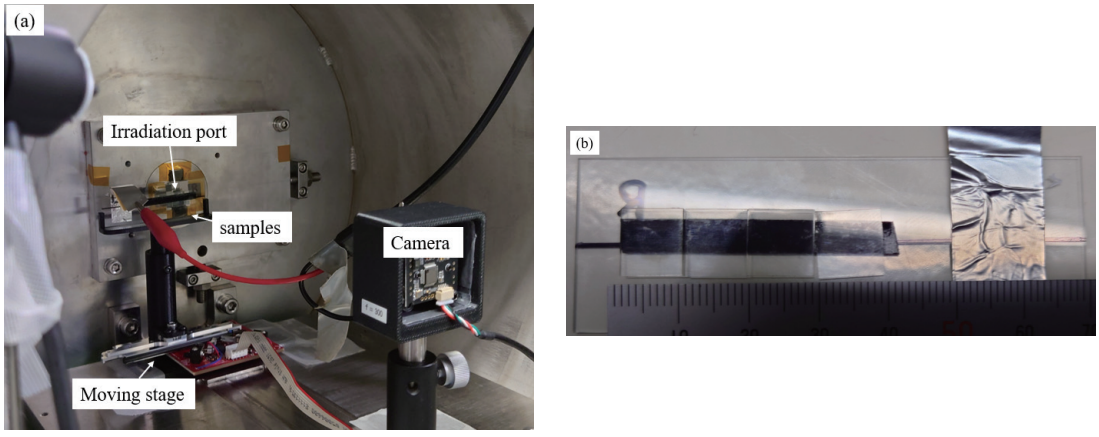

Fig. 1. (Color online) Photograph of (a) an area near the irradiation port and (b) sample setting.

spectra were measured using an ESR spectrometer (JES-X330, JEOL). Samples were cut to fit into an ESR tube with an inner diameter of 4 mm. The ESR measurement conditions were as follows: microwave frequency, 9444 MHz; microwave power, 6.0 mW; modulation field, 0.8 mT; time constant, 0.03 s; amplitude, 1000; scan speed, 4 min; and scan repeat, 4 times.

3. Results and Discussion

Figure 2 shows the appearance of irradiated samples. All the samples were transparent, and a dark brown coloration of the irradiated areas was observed, especially in the samples irradiated with more than 100 Gy.

Figure 3 shows the UV–Vis absorption spectra. In Fig. 3(a), the absorbance in the wide wavelength range (200–700 nm) increased with proton dose. In particular, the broad absorption band peaking at 310 nm appeared after proton irradiation. These results indicate that new absorption centers were formed by proton irradiation. To analyze the detailed reaction, we carried out the Gaussian fitting of optical absorption spectra in the sample irradiated with 10000 Gy. Equation (1) was used to fit the spectra.

$$A(\lambda) = \sum_i A_i \exp\left\{-\frac{(\lambda - b_i)^2}{c_i^2}\right\} \tag{1}$$

Here, $A(\lambda)$ is the absorbance at wavelength λ. A_i, b_i, and c_i are the fitting parameters corresponding to the peak absorbance, peak wavelength, and constant related to the full width at half maximum for component i, respectively. The number of components was determined to be seven on the basis of previous reports.[37,42] The fitting result is shown in Fig. 3(b). The absorption spectra in the 10000-Gy-irradiated sample were fitted well by seven Gaussian functions. On the basis of the b_i values, each band is attributed to PO_3 (6.23 eV), Ag^+ (5.65 eV), Ag_3^{2+} (4.91 eV), Ag_2^+ (4.42 eV), Ag^{2+} (3.84 eV), Ag^0 (3.25 eV), and POHC (2.43 eV). The comparison of peak energies for each peak to previous reports is shown in Table 1. To investigate the proton dose dependence of the number of these absorption centers, we fitted absorption

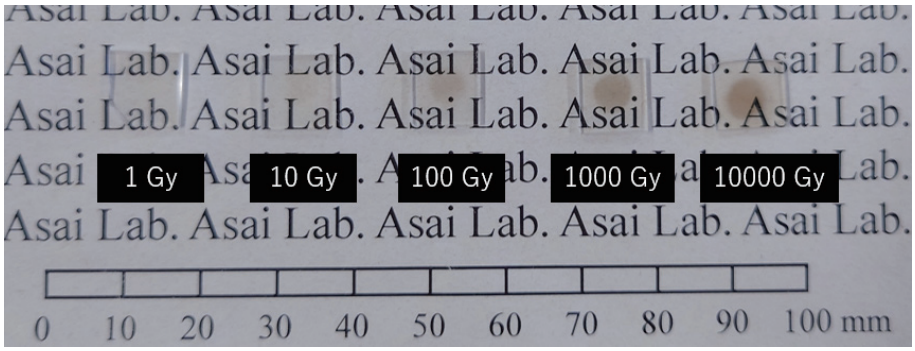

Fig. 2. (Color online) Appearance of irradiated samples.

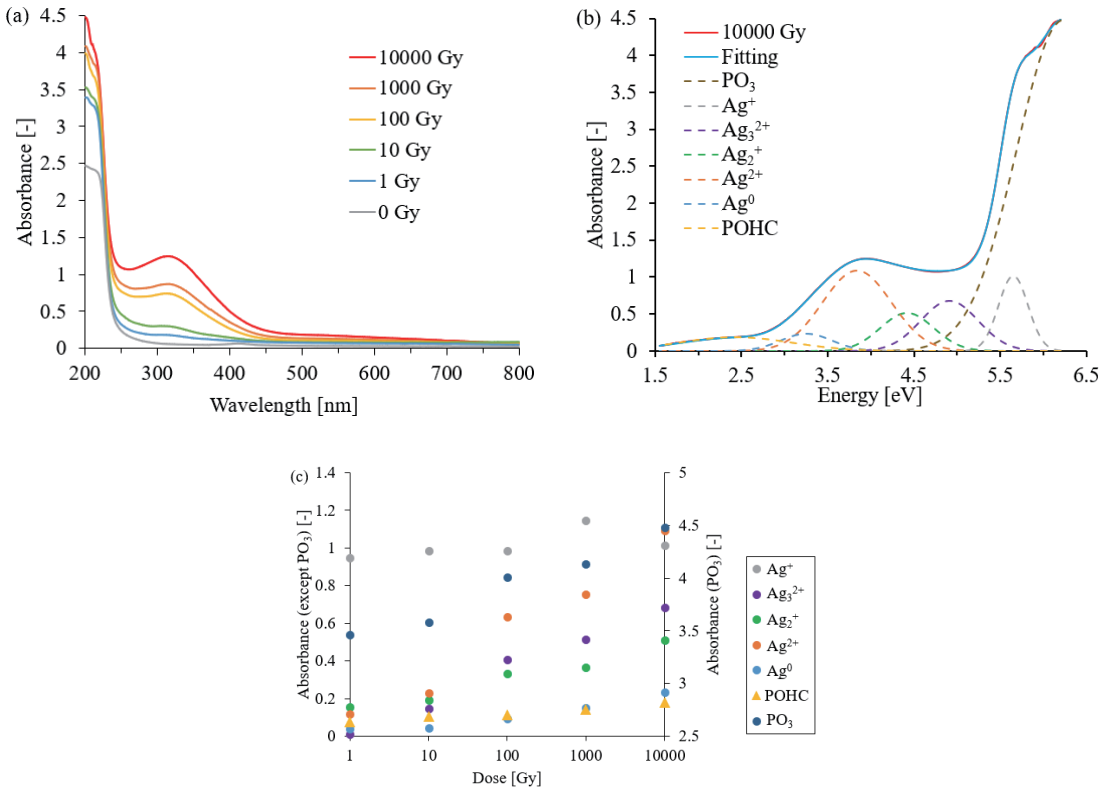

Fig. 3. (Color online) (a) Proton dose dependence of UV–Vis absorption spectra. (b) Fitting result of the spectra in the 10000 Gy irradiated sample. (c) Proton dose dependence of peak absorbance (A_i) of each band.

Table 1
Attribution of absorption bands.

	PO_3	Ag^+	Ag_3^{2+}	Ag^{2+}	Ag^{2+}	Ag^0	POHC	
	6.23	5.65	4.91	4.42	3.84	3.25	2.43	This study
Peak energy (eV)	~6.30	5.39	4.87	4.43	3.94	3.31	–	Ref. 42
		5.23	4.87	4.48	3.99	3.37	2.46	Ref. 37

spectra in the samples irradiated with 1–1000 Gy using Eq. (1) by changing only A_i. Figure 3(c) shows the dose dependence of peak absorbance, that is, A_i, for each absorption center. The absorbance monotonically increased with dose for all absorption centers excluding Ag^+. However, note that the fitting result of the PO_3 absorption band lacks reliability because of incomplete spectral shape owing to the wavelength limitation of the measurement instrument. The increase in absorbance with proton dose indicates that Ag^0, Ag^{2+}, Ag_2^+, Ag_3^{2+}, and POHC were formed by proton irradiation. The formation of Ag^0, Ag_2^+, Ag^{2+}, and POHC can be explained by the well-known[35,36] RPL center formation mechanism in Ag-doped phosphate glass as described in Reactions (1)–(4).

$$Ag^{+} + e^{-} \rightarrow Ag^{0} \quad (1)$$

$$Ag^{0} + Ag^{+} \rightarrow Ag_2^{+} \quad (2)$$

$$PO_4^{3-} + h^{+} \rightarrow hPO_4^{2-}\left(POHC\right) \quad (3)$$

$$POHC + Ag^{+} \rightarrow PO_4^{3-} + Ag^{2+} \quad (4)$$

Furthermore, according to a previous report,[37] it has been proposed that Ag_3^{2+} is formed by the association of Ag_2^{+} and Ag^{+} as shown in Reaction (5).

$$Ag_2^{+} + Ag^{+} \rightarrow Ag_3^{2+} \quad (5)$$

Because Ag^0, Ag^{2+}, Ag_2^{+}, and Ag_3^{2+} are formed by electron and hole capturing and the clustering of Ag^{+} as introduced in Reactions (1)–(5), the absorbance of Ag^{+} should decrease with increasing proton dose. However, no significant change in the absorbance of Ag^{+} was observed. This is considered to be because the absorption band of Ag^{+} was completely covered by that of PO_3, making it difficult to observe a change in absorbance.

Figure 4(a) shows the proton dose dependence of the PL spectra with an excitation wavelength of 310 nm. The excitation wavelength was determined on the basis of the result of UV–Vis absorption spectra [Fig. 3(a)]. As shown in Fig. 3(b), absorption bands of Ag^{2+} and Ag_2^{+} covered 310 nm (4.00 eV). Hence, 310 nm light was considered to be exciting mainly Ag^{2+} and Ag_2^{+}. In Fig. 4(a), a broad emission band peaking at 650 nm was observed in the proton-irradiated samples. This emission is the well-known orange RPL in Ag-doped phosphate glass.[31–36] Considering the chemical species excited by 310 nm light, Ag^{2+} and Ag_2^{+} are considered to be RPL centers in this glass, which coincide with previous reports. [35,37] Figure 4(b) shows PLE spectra with an emission wavelength of 650 nm. Excitation peaks at approximately 280 and 310 nm were induced by proton irradiation. As shown in a previous report,[35] the excitation peaks at 280 and 310 nm are attributed to Ag_2^{+} and Ag^{2+}, respectively. Hence, this result also suggests the formation of Ag_2^{+} and Ag^{2+} by proton irradiation. Figure 4(c) shows the proton dose dependence of emission intensity at 650 nm. The intensity increased up to 10 Gy and decreased in the dose range larger than 100 Gy. The increase in emission intensity corresponds to increases in the amounts of Ag_2^{+} and Ag^{2+} by proton irradiation. To discuss the reason for the decreasing emission intensity in the high dose range, we focused on Figs. 2 and 3(c). As shown in Fig. 2, the irradiated area was apparently colored dark brown in the samples irradiated with more than 100 Gy. Therefore, it is considered that the effect of self-absorption was more pronounced in the samples irradiated with doses of 100 Gy or more. In particular, the absorption of RPL emission by POHC may occur because the absorption band of POHC overlaps with the RPL emission wavelength. In addition, the amounts of Ag^{2+} and Ag_2^{+} monotonically increased with proton dose as shown in Fig. 3(c). Hence, the effect of concentration quenching is also possible.

Figure 5 shows the ESR spectra, and the observed signals are summarized in Table 2. In all the samples including the unirradiated sample (0 Gy), the signal at approximately 350 mT (g =

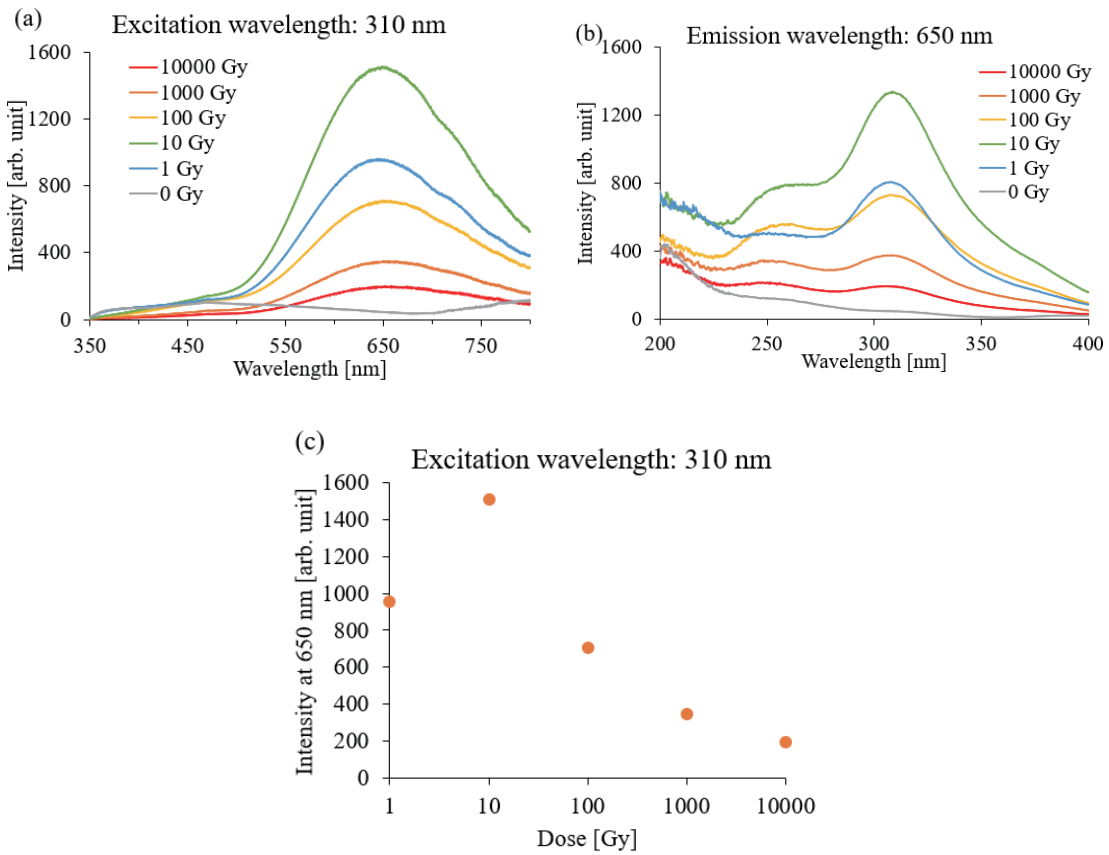

Fig. 4. (Color online) Proton dose dependence of (a) PL and (b) PLE spectra. (c) Proton dose dependence of emission intensity at 650 nm.

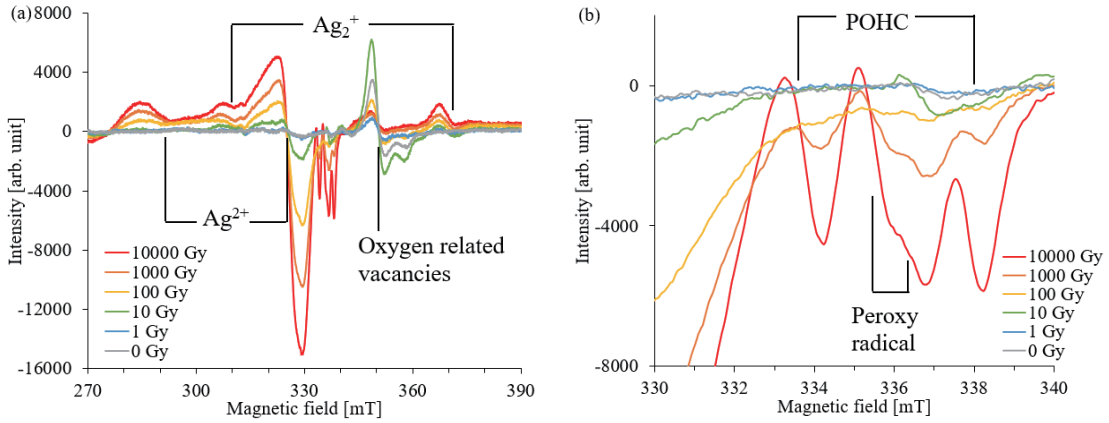

Fig. 5. (Color online) (a) Proton dose dependence of ESR spectra. (b) Enlarged figure of ESR spectra around 330–340 mT.

1.924) was observed. On the basis of a previous report,[46] this signal is attributed to ^{16}O-related vacancies. The ESR signal of oxygen-related vacancies was observed from 0 Gy, whereas no significant emission peak was observed in the PL spectra of the unirradiated sample. This result clearly indicates that the oxygen-related vacancies did not contribute to RPL emission. In this

Table 2
ESR signals induced by proton irradiation.

Paramagnetic species	Magnetic field (mT)	*g*-value in this study (-)	*g*-value in reference (-)	Reference number
Ag^{2+}	289 325	2.329 2.073	$g_{\parallel}$: 2.373 $g_{\perp}$: 2.054	46
Ag_2^{+}	309, 370	2.183, 1.823 mean: 2.003	1.986	47
POHC	334, 338	2.002, 1.996 mean: 1.999	2.009	48
Peroxy-radical	335 336	2.009 2.004	2.010 2.005	50

study, different samples were irradiated with different doses, so it is not possible to determine whether the change in the signal intensity of oxygen-related vacancies was due to a proton dose increase or individual differences between samples. However, in our previous study,[46] no significant change in the signal intensity of oxygen-related vacancies was observed in the same Ag-doped phosphate glass before and after 1000 Gy of X-ray irradiation. Therefore, the oxygen-related vacancies are not considered to be involved in RPL. Because our objective is to elucidate the proton irradiation effect in Ag-doped Na–Al phosphate glasses, we focused on the signals induced by proton irradiation below. The ESR signals were observed at approximately 289, 309, 325, 335, and 370 mT. According to previous reports,[46,47] the signals at 289 (g = 2.329) and 325 mT (g = 2.073) are attributed to Ag^{2+}. In addition, the signals at 309 (g = 2.183) and 370 mT (g = 1.823), with a mean g-value of 2.003, are attributed to Ag_2^{+}.[46,48] These results indicate the formation of Ag^{2+} and Ag_2^{+}, which coincides with the result of UV–Vis absorption and PL/PLE spectroscopies. Ag^{2+} is formed by the hole trapping of Ag^{+}, whereas Ag_2^{+} is formed by the association of Ag^{+} and Ag^{0} formed by the electron trapping of Ag^{+}. Hence, some of the electrons and holes generated by proton irradiation were trapped by Ag^{+}. Focusing on the signal around 335 mT [Fig. 5(b)], we observed four signals at 334, 335, 336, and 338 mT in the samples irradiated with more than 1000 Gy. From the g-values previously reported, the signals at 334 (g = 2.002) and 338 mT (g = 1.996), with a mean g-value of 1.999, are attributed to POHC.[34,46,49] POHC is a hole trapped at PO_4^{3-} tetrahedra. Therefore, this result indicates that some of the holes generated by proton irradiation were trapped at not only Ag^{+} but also PO_4^{3-} tetrahedra. In addition, the signals at 335 (g = 2.009) and 336 (g = 2.004) are attributed to peroxy-radicals,[50–52] which are trapped holes on oxygen atoms at the end of a short chain ($-P-O-O\cdot$). Interestingly, the signal of peroxy-radical was observed in the samples irradiated with more than 1000 Gy of protons in this study, whereas in previous studies, the signal of peroxy-radical was not observed in Ag-doped phosphate glasses irradiated with 1 kGy of X-rays,[46] 1.5 kGy of β-rays,[35] and 10^4 and 10^6 Gy of electron beams.[52] Therefore, no peroxy-radicals were formed in Ag-doped phosphate glasses when exposed to low-LET radiation but were formed when exposed to high-LET proton irradiation. In a previous report,[52] it was proposed that high doses lead to a structural change in the host glass and promote the formation of $-P-O-O$ bonds. Because high-LET radiation deposits a large amount of energy per unit length, there may be areas where a large amount of energy has been deposited locally, and $P-O-O$ may have been formed in those areas. However, to the best of our knowledge, there

are no reports indicating the ESR signal of peroxy-radical in Ag-doped phosphate glasses. Hence, further investigations, such as the effect of proton irradiation on nondoped phosphate glasses, are needed to confirm that the signals observed at 335 and 335 mT originate from peroxy-radicals.

4. Conclusions

In this study, we investigated UV–Vis absorption, PL/PLE, and ESR spectra in proton-irradiated Ag-doped Na–Al phosphate glass to elucidate the proton irradiation effect in this glass. The formation of Ag^0, Ag^{2+}, Ag_2^+, Ag_3^{2+}, and POHC by proton irradiation was suggested by UV–Vis absorption spectra. The amount of these chemical species formed increased monotonically with proton dose. In PL/PLE spectra, a new emission band at 650 nm and excitation bands at 280 and 310 nm appeared after proton irradiation corresponding to the formation of Ag^{2+} and Ag_2^+. The PL intensity at 650 nm increased up to 10 Gy and decreased in the dose range larger than 100 Gy. This decrease in PL intensity with proton dose was considered to be induced by self-absorption and concentration quenching. In ESR spectra, the ESR signals of Ag^{2+}, Ag_2^+, POHC, and peroxy-radicals were observed in proton-irradiated samples. In particular, the formation of peroxy-radical is considered to be interesting because this reaction was not observed in Ag-doped phosphate glasses irradiated with low-LET radiation in previous reports. However, it is not possible to determine with certainty whether peroxy-radicals are the cause of LET quenching based on only these results. Therefore, we plan to analyze the behavior of RPL emission and RPL center formation when irradiated with high- or low-LET radiation and investigate the LET dependence of the ESR spectra in future work.

Acknowledgments

This work was supported by a Grant-in Aid for Scientific Research (A) (Grant No. 22H00308, 2022–2026), a Grant-in-Aid for Challenging Research (Exploratory) (Grant No. 24K21544, 2024–2026), and a Grant-in-Aid for Scientific Research (B) (Grant No. 25K01702, 2025–2028) funded by the Japan Society for the Promotion of Science, the Kato Foundation for the Promotion of Science 2025 research grant, and the Amano Institute of Technology 2024 research grant, respectively. We thank Dr. S. Hatori, Dr. T. Kurita, and the accelerator group for supplying the high-quality beam. We also thank Mr. K. Uda for supporting our beam irradiation experiments.

References

1 J. A. Perry: RPL Dosimetry: Radiophotoluminescence in Health Physics (Adam Hilger, Bristol, U.K., 1987) p. 3.
2 D. Y. C. Huang and S. M. Hsu: Advances in Center Therapy, H. G. Muhtasib Ed. (IN Tech, Rijeka, 2011) p. 553.
3 K. Nomura, T. Ikegami, and N. Juto: Radioisotopes **51** (2002) 85 (in Japanese). https://doi.org/10.3769/radioisotopes.51.85
4 S. Koyama, Y. Miyamoto, A. Fujiwara, H. Kobayashi, K. Ajisawa, H. Komori, Y. Takei, H. Nanto, T. Kurobori, H. Kakimoto, M. Sakakura, Y. Shimotsuma, K. Miura, K. Hirao, and T. Yamamoto: Sens. Mater. **22** (2010) 377. https://doi.org/10.18494/SAM.2010.690
5 H. Nanto, Y. Miyamoto, T. Oono, Y. Takei, T. Kurobori, and T. Yamamoto: Procedia Eng. **25** (2011) 231. https://doi.org/10.10.1016/j.prpeng.2011.12.057

6 Z. Knezevic, N. Beck, D. Milkovic, S. Miljanic, and M. Ranogajec-Komor: Radiat. Meas. **46** (2011) 1582. https://doi.org/10.1016/j.radmeas.2011.05.042
7 T. Kurobori and S. Nakamura: Radiat. Meas. **47** (2012) 1009. https://doi.org/10.1016/j.radmeas.2012.09.003
8 T. Kurobori, A. Takemura, Y. Miyamoto, D. Maki, Y. Koguchi, N. Takeuchi, T. Yamamoto, and Y. Q. Chen: Radiat. Meas. **83** (2015) 51. https://doi.org/10.1016/j.radmeas.2015.04.017
9 T. Yanagida, G. Okada, T. Kato, D. Nakauchi, and N. Kawaguchi: Radiat. Meas. **158** (2022) 106847. https://doi.org/10.1016/j.radmeas.2022.106847
10 F. Nakamura, T. Kato, G. Okada, N. Kawaguchi, K. Fukuda, and T. Yanagida: Ceram. Int. **43** (2017) 7211. https://doi.org/10.1016/j.ceramint.2017.03.009
11 T. Kato, D. Nakauchi, N. Kawaguchi, and T. Yanagida: Mater. Lett. 270 (2020) 127688. https://doi.org/10.1016/j.matlet.2020.127688
12 F. Nakamura, T. Kato, G. Okada, N. Kawano, N. Kawaguchi, and T. Yaganida: Mater. Lett. **221** (2018) 51. https://doi.org/10.1016/j.matlet.2018.03.080
13 F. Nakamura, T. Kato, D. Nakauchi, G. Okada, N. Kawano, N. Kawaguchi, and T. Yanagida: Chem. Lett. **46** (2017) 1383. https://doi.org/10.1246/cl.170580
14 G. Okada, Y. Koguchi, T. Yanagida, and H. Nanto: Mater. Today Commun. **24** (2020) 101013. https://doi.org/10.1016/j.mtcomm.2020.101013
15 D. Shiratori, H. Kimura, Y. Fukuchi, and T. Yanagida: Sens. Mater. **36** (2024) 547. https://doi.org/10.18494/SAM4764
16 H. Kawamoto, Y. Fujimoto, and K. Asai: Radiat. Meas. **179** (2024) 107320. https://doi.org/10.1016/j.radmeas.2024.107320
17 H. Tanaka, Y. Fujimoto, M. Koshimizu, T. Yanagida, T. Yahaba, K. Saeki, and K. Asai: Sens. Mater. **28** (2016) 863. https://doi.org./10.18494/SAM.2016.1246
18 A. Nishikawa, D. Shiratori, T. Kato, D. Nakauchi, N. Kawaguchi, and T. Yanagida: Radiat. Meas. **170** (2024) 107052. https://doi.org/10.1016/j.radmeas.2023.107052
19 H. W. Etzel, J. H. Schulman, R. J. Ginther, and E. W. Claffy: Phys. Rev. **85** (1952) 1063. https://doi.org/10.1103/PhysRev.85.1063
20 H. Kawamoto, Y. Fujimoto, and K. Asai: Sens. Mater. 36 **2** (2) (2024) 607. https://doi.org/10.18494/SAM4766
21 R. Morishita, H. Kawamoto, Y. Fujimoto, and K. Asai: J. Lumin. **288** (2025) 121563. https://doi.org/10.1016/j.jlumin.2025.121563
22 R. Hashikawa, Y. Fujii, A. Kinomura, T. Saito, A. Okada, T. Wakasugi, and K. Kadono: J. Am. Ceram. Soc. 102 **4** (2019) 1642. https://doi.org/10.1111/jace.16027
23 Y. Fujimoto, G. Okada, D. Sekine, T. Yanagida, M. Koshimizu, H. Kawamoto, and K. Asai: Radiat. Meas. **133** (2020) 106274. https://doi.org/10.1016/j.radmeas.2020.106274
24 G. Okada, W. Shinozaki, S. Ueno, Y. Koguchi, K. Hirasawa, F. D'Errico, T. Yanagida, S. Kasap, and H. Nanto: Jpn. J. Appl. Phys. **61** (2022) SB1035. https://doi.org/10.35848/1347-4065/ac1ab2
25 A. Nishikawa, D. Shiratori, T. Kato, D. Nakauchi, N. Kawaguchi, and T. Yanagida: **36** (2024) 597. https://doi.org/10.18494/SAM4755
26 C. Pandey, S. M. Dhopte, P. L. Muthal, V. K. Kondawar, and S. V. Moharil: Radiat. Eff. Defects Solids **162** (2007) 651. https://doi.org/10.1080/10420150701197547
27 H. Nalumaga, J. J. Schuyt, and G. V. M. Williams: Opt. Mater. **157** (2024) 116192. https://doi.org/10.1016/j.optmat.2024.116192
28 J. J. Schuyt, G. V. M. Williams, and S. V. Chong: Opt. Mater. **133** (2022) 112926. https://doi.org/10.1016/j.optmat.2022.112926
29 T. Nakamura, G. Okada, and H. Nanto: J. Alloys Compd. **979** (2024) 173498. https://doi.org/10.1016/j.jallcom.2024.173498
30 G. Okada, C. O. Fernandes, H. Ito, Y. Koguchi, S. Ueno, C. Sawai, W. Kada, K. Watanabe, K. Shinsho, and H. Nanto: Sens. Mater. **37** (2025) 533. https://doi.org/10.18494/SAM5440
31 J. H. Schulman, R. J. Ginther, and C. C. Klick: J. Appl. Phys. **22** (1951) 1479. https://doi.org/10.1063/1.1699896
32 R. Yokota and H. Imagawa: J. Phys. Soc. Jpn. **23** (1967) 1038. https://doi.org/10.1143/JPSJ.23.1038
33 T. Kurobori, W. Zheng, Y. Miyamoto, H. Nanto, and T. Yamamoto: Opt. Mater. **32** (2010) 1231. https://doi.org/10.1016/j.optmat.2010.04.004
34 Y. Miyamoto, Y. Takei, H. Nanto, T. Kurobori, A. Konnai, T. Yanagida, A. Yoshikawa, Y. Shimotsuma, M. Sakakura, K. Miura, K. Hirao, Y. Nagashima, T. Yamamoto: Radiat. Meas. **46** (2011) 1480. https://doi.org/10.1016/j.radmeas.2011.05.048
35 S. W. S. Mckeever, S. Sholom, and N. Shrestha: Radiat. Meas. **123** (2019) 13. https://doi.org/10.1016/j.radmeas.2019.02.009

36 H. Kawamoto, M. Koshimizu, Y. Fujimoto, and K. Asai: Jpn, J. Appl. Phys. **62** (2023) 010501. https://doi.org/10.35848/1347-4065/ac9cb0
37 S. Sholom, and S. W. S. McKeever: Radiat. Meas. **163** (2023) 106924. https://doi.org/10.1016/j.radmeas.2023.106924
38 Y. Miyamoto, H. Nanto, T. Kurobori, Y. Fujimoto, T. Yanagida, J. Ueda, S. Tanabe, and T. Yamamoto: Radiat. Meas. **71** (2014) 529. https://doi.org/10.1016/j.radmeas.2014.08.007
39 H. Yasuda and K. Fujitaka: Radiat. Prot. Dosim. **87** (2000) 115. https://doi.org./10.1093/oxfordjournals.rpd.a032983
40 M. Majer, L. Pasariček, Ž. Knežević, T. Bokulić, G. Provatas, and I. B. Mihalić: Radiat. Meas. **166** (2023) 106973. https://doi.org/10.1016/j.radmeas.2023.106973
41 T. Kurobori, Y. Yanagida, S. Kodaira, and T. Shirao: Nucl. Instrum. Methods Phys. Res. A. **855** (2017) 25. https://doi.org/10.1016/j.nima.2017.02.057
42 T. Kurobori, Y. Miyamoto, N. Takashima, Y. Kitagawa, and Y. Koguchi: Radiat. Meas. **181** (2025) 107376. https://doi.org/10.1016/j.radmeas.2025.107376
43 S. Hatori, R. Ishigami, K. Kume, and K. Suzuki: Quantum Beam Sci. **5** (2021) 14. https://doi.org/10.3390/qubs5020014
44 K. Suzuki, and B. Tsuchiya: Nucl. Instrum. Methods Phys. Res. B **554** (2024) 165413. https://doi.org/10.1016/j.nimb.2024.165413
45 J. F. Ziegler, J. P. Biersack, and U. Littmark: The Stopping and Range of Ions in Solids (Pergamon, Oxford, UK, 1985).
46 H. Kawamoto, Y. Fujimoto, and K. Asai: J. Lumin. **288** (2025) 121562. https://doi.org/10.1016/j.jlumin.2025.121562
47 P. Balaya and C. S. Sunandana: Solid State Ionics **40** (1990) 700. https://doi.org/10.1016/0167-2738(90)90102-W
48 N. I. Mel'nikov, D. P. Peregood, and R. A. Zhitnikov: J. Non-Cryst. Solids **16** (1974) 195. https://doi.org/10.1016/0022-3093(74)90124-0
49 P. Ebelng, D. Ehrt, and M. Friedrich: Opt. Mater. **20** (2002) 101. https://doi.org/10.1016/S0925-3467(02)00052-6
50 M. E. Archidi, M. Haddad, A. Nadiri, F. Benyaich, and R. Berger: Nucl. Instr. And Meth. In Phys. Res. B **116** (1996) 145. https://doi.org/10.1016/0168-583X(96)00026-2
51 V. Pukhkaya, F. Trompier, and N. Ollier: J. Appl. Phys. **116** (2014) 123517. https://doi.org/10.1063/1.4896876
52 F. Alassani, J. C. Desmoulin, O. Cavani, Y. Petit, T. Cardinal, and N. Ollier: J. Non Cryst. Solids **600** (2023) 122009. https://doi.org/10.1016/j.jnoncrysol.2022.122009